Hindawi Publishing Corporation
International Journal of Photoenergy
Volume 2013, Article ID 560840, 10 pages
http://dx.doi.org/10.1155/2013/560840

Research Article

Photoactive TiO_2 Films Formation by Drain Coating for Endosulfan Degradation

Natalia Tapia-Orozco[1] and Refugio Rodríguez Vázquez[1,2]

[1] *Programa de Nanociencias y Nanotecnología, Centro de Investigación y de Estudios Avanzados del Instituto Politécnico Nacional, Ave Instituto Politécnico Nacional 2508, San Pedro Zacatenco, 07360 Mexico City, DF, Mexico*
[2] *Departamento de Biotecnología y Bioingeniería, Centro de Investigación y de Estudios Avanzados del Instituto Politécnico Nacional, Ave. Instituto Politécnico Nacional 2508, San Pedro Zacatenco, 07360 Mexico City, DF, Mexico*

Correspondence should be addressed to Refugio Rodríguez Vázquez; rrodrig@cinvestav.mx

Received 22 February 2013; Accepted 30 April 2013

Academic Editor: Ewa Kowalska

Heterogeneous photocatalysis is an advanced oxidation process in which a photoactive catalyst, such as TiO_2, is attached to a support to produce free radical species known as reactive oxygen species (ROS) that can be used to break down toxic organic compounds. In this study, the draining time, annealing temperature, and draining/annealing cycles for TiO_2 films grown by the drain coating method were evaluated using a 2^3 factorial experimental design to determine the photoactivity of the films via endosulfan degradation. The TiO_2 films prepared with a large number of draining/annealing cycles at high temperatures enhanced ($P > 0.05$) endosulfan degradation and superoxide radical generation after 30 minutes of illumination with UV light. We demonstrated a negative correlation ($R^2 = 0.69$; $P > 0.01$) between endosulfan degradation and superoxide radical generation. The endosulfan degradation rates were the highest at 30 minutes with the F6 film. In addition, films prepared using conditions F1, F4, and F8 underwent an adsorption/desorption process. The kinetic reaction constants, K_{app} (min^{-1}), were 0.0101, 0.0080, 0.0055, 0.0048, and 0.0035 for F6, F2, F5, F3, and F1, respectively. The endosulfan metabolites alcohol, ether, and lactone were detected and quantified at varying levels in all photocatalytic assays.

1. Introduction

In advanced oxidation processes (AOPs), the use of heterogeneous photocatalysis has been extensively studied for the removal of wastewater pollutants [1–5]. One of the main advantages of heterogeneous photocatalysis is dispensing with photocatalyst recuperation, as the photocatalyst has been immobilized on a solid support. This immobilization leads to high pollutant mineralization, minimal waste disposal problems, low cost, and mild temperature and pressure conditions [6]. One of the toxic compounds used to determine the photoactive effect of the catalysis process is the pesticide endosulfan, an organochlorine compound (OC) commonly detected in water and air that is composed of α and β isomers (αE and βE). This pollutant is known to undergo bioaccumulation and biomagnification in food chains [7], and it is widely used for agricultural purposes due to its effective toxicological action and relatively low environmental persistence relative to other organochlorine pesticides. As mentioned earlier, a set of international guidelines and recommendations has been established to restrict or prohibit the use of this pesticide and to further the elimination of current supplies. AOPs are an alternative means of degrading OCs, which are photosensitive and are therefore subjected to natural environmental attenuation; however, this process can take more than two months [8]. Reduction of these toxic organic compounds can be enhanced by using photoactive catalysts; therefore, preparation of these catalysts is important. Photocatalysis can be accomplished by materials that are able to catalyze light-mediated reactions without self-consumption. Semiconductor materials have photoactive properties, are photo stable and nontoxic and are biologically and chemically inert, making them excellent photocatalysts for AOPs [6]. Among the most used catalysts,

which also include ZnO, CeO_2, CdS, and ZnS, titanium dioxide (TiO_2) results in the highest quantum yields. [9, 10]. The main reactions occurring during TiO_2 photocatalysis are the following [11, 12]:

$$TiO_2 + h\nu \longrightarrow e^- + h^+ \quad (1)$$

$$(O_2)_{ads} + e^- \longrightarrow (O_2^{-\bullet})_{ads} \quad (2)$$

$$Ti\,(IV)\text{-}OH + h^+ \longleftrightarrow Ti\,(IV)\text{-}{}^{\bullet}OH \quad (3)$$

$$Ti\,(IV)\text{-}OH_2 + h^+ \longleftrightarrow Ti\,(IV)\text{-}{}^{\bullet}OH + H^+. \quad (4)$$

Reaction (1) involves semiconductor irradiation with light ($>E_g$) to generate an (e^-/h^+) pair such that the electron is in the conduction band and the hole is in the valence band. The band gap energy (E_g) of titanium oxide is 3.2 eV [9]. The (e^-/h^+) pair will then initiate the oxidation and reduction processes of adsorbed substrates. Molecular oxygen (O_2) is adsorbed at Ti(III) surface sites, which reduce the oxygen to the superoxide anion radical ($O_2^{-\bullet}$) (Reaction (2)). The Ti(IV)-$O^{-\bullet}$-Ti(IV) complex oxidizes the surface hydroxyl groups or the surface-bound water to hydroxyl radicals ($^{\bullet}OH$), which also occurs on the semiconductor surface (Reactions (3) and (4)) [13, 14].

Heterogeneous photocatalysis can be carried out in the gaseous phase, the pure organic liquid phase, and in aqueous solutions. Herrmann [9] suggests that heterogeneous catalysis occurs in the following stages: (1) reactant transfer through the catalyst surface, (2) reactant adsorption, (3) reaction in the adsorbed phase, (4) product desorption, and (5) product removal in the interfacial region.

Several physical and chemical approaches have been considered for the preparation of photoactive TiO_2 films. In particular, the chemical processes known as wet methods are very popular because they consume less energy and do not require vacuum equipment, thus resulting in a low-cost system preparation. This type of deposition is performed through a colloidal solution and a subsequent annealing process to improve pollutant photodegradation; adhesion of the titanium substrate allows for an increase in electric conductivity [15]. The photocatalytic activity of grid-like mesoporous TiO_2 films has been correlated with the physical properties of these films, such as crystallinity, pore size, and accessibility, the ratio of anatase to rutile isomers, and other properties [16]. However, other conditions might affect the properties of the photoactive catalysts, such as the type of methodology and the conditions for TiO_2 film preparation.

The aim of this study is to elucidate appropriate conditions for photoactive TiO_2 film preparation on a glass substrate and to test these catalysts through endosulfan pesticide degradation.

2. Experimental Methods

2.1. Reagents. The following analytical-grade reagents were employed without further purification: nitric acid (HNO_3), hydrogen peroxide (H_2O_2), absolute ethanol, and titanium isopropoxide. The commercial endosulfan pesticide with a minimal concentration of 35% was kindly donated by an agricultural company and contained an α : β endosulfan ratio of approximately 60 : 40 and a total endosulfan concentration of 625.7 mg L^{-1}. An endosulfan standard (59.2% α + 39.9% β) was employed. The endosulfan metabolite standards alcohol, ether, and lactone were employed. HPLC-grade solvents, including hexane and dichloromethane were used for pesticide extraction and quantification. Colloidal films were prepared with powdered nanoparticles of TiO_2 with a size of ~21 nm and ≥99.5% trace metal basis. Sterile deionized water (pH = 4.0 bar, W 45%) was employed for the treatment studies.

Table 1: Matrix of the 2^3 factorial experimental design for film formation, in natural values.

Films conditions	Draining/annealing cycles	Draining time (h)	Annealing temperature (°C)
F1	1	2	450
F2	2	2	450
F3	1	3	450
F4	2	3	450
F5	1	2	550
F6	2	2	550
F7	1	3	550
F8	2	3	550

2.2. Colloidal Solution Preparation. TiO_2 nanoparticle deposition was performed according to the drain coating method. The colloidal solution was prepared from two primary solutions; the first solution consisted of TiO_2 nanoparticles (4.7 mM), HNO_3 (4.71 mM) and deionized water. The second solution was prepared with H_2O_2 (0.68 mM), titanium isopropoxide (0.68 mM) and absolute ethanol [17]. The two solutions were mixed and sonicated for 5 minutes. The resulting solution was maintained in the absence of light under freezing conditions.

2.3. Substrate. Plates of sodalime glass were employed as a substrate for TiO_2 films. The predeposition cleaning process for the plates consisted of sonication first in distilled water and then in ethanol, acetone, and, finally, deionized water. The product was air dried.

2.4. Photoactive TiO_2 Film Preparation. A 2^3 factorial experimental design was proposed. The three factors evaluated were draining/annealing (1 or 2 cycles), draining time (2 or 3 hours), and annealing temperature (450 or 550°C). The experimental matrix consisted of 8 runs (Table 1), each of which was performed in triplicate.

2.5. Photoactivity Assays of TiO_2/UV through Endosulfan Degradation. The photo reactor for this study was a Foto Q 200, Mexico, with a nominal volume of 1 L and an effective volume of 600 mL. It included a fluorescent mercury vapor lamp (254 nm) operating at 60 watts. The UV lamp has

a water cooling system, which was maintained at 15°C ± 2. The TiO_2 film plates with a size of 7.5 × 2.5 cm were set in an inert *Teflon* support inside a photo reactor. The initial pH of the endosulfan solution was 6.0 and this was not adjusted. Sampling was performed every 30 minutes for 2.5 hours. The presence of superoxide radicals was determined as described by Bolwell et al. [18]; the dissolved oxygen (DO) concentration was measured using the NMX-AA-012-SCFI-2001 technique [19]. Endosulfan isomers and metabolites were analyzed on a Varian CP-3380 gas chromatograph (USA) equipped with an electron capture detector; 1 μL aliquots of the sample extracts were injected into a fused-silica capillary column (5CB Varian, 15 m × 0.25 mmID). Nitrogen was used as the carrier and make-up gas at a column flow of 3.5 mL min^{-1}. The injector and detector temperatures were 200 and 300°C, respectively. The oven temperature was maintained at 80°C for 1 min and then increased at a rate of 20°C min^{-1} to 200°C over a period of 8 min. The chromatographic software employed was Galaxie Workstation. The identification and quantitative analysis of parental compound samples and metabolites were accomplished using a calibration curve for each component using analytical standards of endosulfan (α + β), alcohol, ether, and lactone endosulfan.

Each treatment was performed with a 0.0102 mg L^{-1} commercial endosulfan solution in 600 mL of sterile deionized water. All photo reactor glass accessories were sterilized, but the assays were not performed under sterile conditions. Each experimental run was performed in triplicate, and the results were statistically analyzed using an ANOVA, a least standard deviation and regression models implemented in SAS System 9.0 and Design Expert 6.0.6.

2.5.1. Dark Phase Control (TiO_2). The 2^3 factorial experimental design described in Section 2.4 was evaluated without UV radiation. Each run was performed over a period of 5 hours; samples were collected every 30 minutes during the first 2 hours and then hourly between hours 2 and 5. Each run was performed at 15°C ± 2. The superoxide radical intensity and DO values were determined, and the parental compounds and metabolites pesticide were identified and quantified as described in Section 2.5, and a statistical analysis was performed. Endosulfan volatilization was performed by solid-phase microextraction (SPME) with a 100 μm polydimethylsiloxane microfiber and an SPME fiber holder. The photoreactor was covered with a parafilm septum, and external UV irradiation was avoided. The standard microextraction exposition time on microfiber was 45 seconds in the photoreactor headspace and 5 minutes inside the GC-ECD injector. The 2 μL microfiber volume was calculated according to the method of Hinshaw [20]. Meanwhile, the headspace extraction volume was approximately 376.99 mL.

2.5.2. Photolysis Control (UV). This treatment was performed in the absence of TiO_2-deposited plates at 15°C ± 2 with an initial concentration of 0.0102 mg L^{-1} commercial endosulfan in 600 mL of sterile deionized water. All of the photo reactor glass accessories were sterilized, but experiments were not performed under sterile conditions. Sampling during the assay was performed every 30 minutes for 2.5 hours. The superoxide radical intensity and DO values were determined, and the parental compounds and metabolite pesticides were identified and quantified as described in Section 2.5.

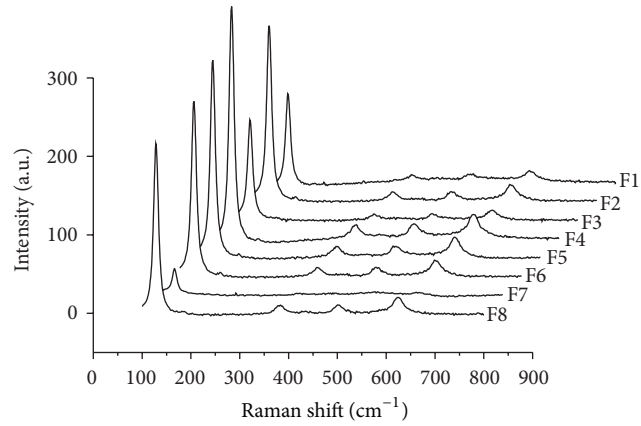

Figure 1: Raman spectra of TiO_2 films formed using the 2^3 experimental design.

2.6. Characterization of TiO_2 Films. The titanium dioxide anatase structure was evaluated using a Thermo Scientific DXR Raman Microscope (USA) with a CCD detector. The 780 nm laser was focused on the film using an optical Olympus microscope with an objective lens magnification of 10x. The laser power was 4 mW, and a 50 μm slit aperture was used; the spectra of the samples were registered with an additional 50 scans. Instrument control and data acquisition were achieved with OMNIC Software. The crystalline structure of the films was analyzed by means of X-ray diffraction (XRD) using a Siemens D-5000 diffractometer with wavelength radiation of 1.5406 Å (Cu kα). The films XRD refinement was performed in PowderCell 2.4 software.

The TiO_2 film thickness was determined using a profilometer Veeco Dektak 6 M Stylus Profiler (USA) equipped with a 12 μm diamond stylus. A scanning distance of 2 mm and a stylus force of 8 mg were used. The instrument control and data acquisition were accomplished with JJPPB-Multi mp software.

3. Results and Discussion

3.1. Characterization of TiO_2 Films. The Raman spectra of the TiO_2 films prepared by 2^3 factorial experimental design are shown in Figure 1 and exhibit bands characteristic of anatase at 645, 512, 395, and 143 cm^{-1} [21]. Except for film F7, these bands were detected in all films prepared, and significant intensity differences apart from F5 and F4 were observed.

The crystallinity of anatase phase was confirmed by XRD analysis (Figure 2), where this photoactive phase was present in all films. The anatase percentage in each film is showed above Miller index anatase (101). However, rutile amount was below than 10%. Specifically, it was possible to confirm the anatase phase in F7 film by XRD pattern,

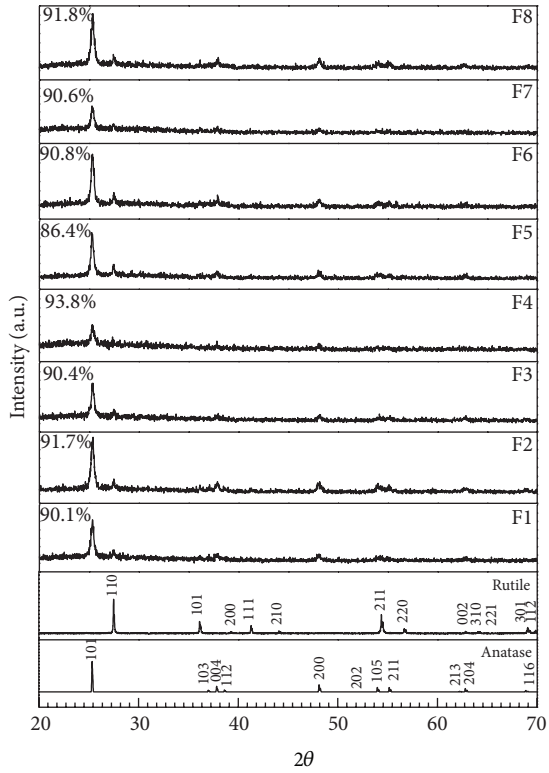

Figure 2: XRD patterns of TiO_2 films formed using the 2^3 experimental design. The reference anatase and rutile patterns were obtained from RRUFF R060277 and RRUFF R040049, respectively.

Table 2: Average thickness of TiO_2 films formed using the 2^3 experimental design.

Run	Thickness (μm)
F1	4.77
F2	2.02
F3	13.82
F4	8.39
F5	4.29
F6	8.21
F7	—
F8	Layer 1 = 9.93 Layer 2 = 7.26

since all characteristic bands in Raman spectrum were not appreciated. In both studies, no effect of temperature in crystallinity phases was observed.

The profile measurements in the films were between 2.02 and 13.82 μm (Table 2), and the F7 film showed considerable roughness such that the thickness could not be determined. These data support the results from the Raman spectrum where no characteristic anatase bands for sample F7 were observed and XRD spectra showed the lowest anatase peaks intensities. Thus, we can conclude that the decrease in pollutant concentration can be attributed to photolysis and not to the TiO_2/UV photoactive system.

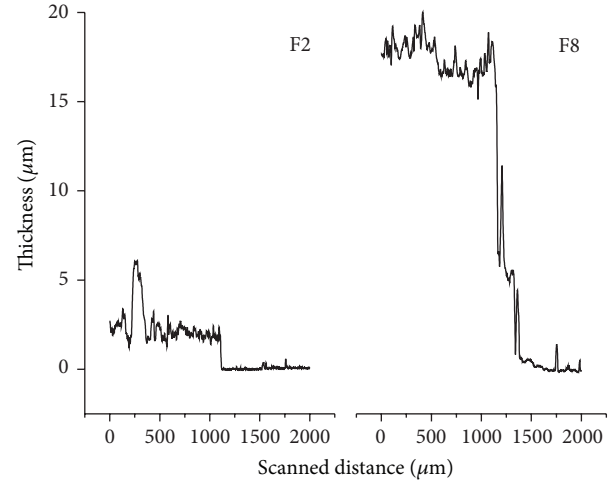

Figure 3: Profilometry of film F2 (2 cycles of draining/annealing, 2 h draining time and 450°C annealing temperature) and film F8 (2 cycles of draining/annealing, 3 h draining time and 550°C annealing temperature).

Figure 3 shows the F2 and F8 film profilometries, where the largest peak represents the greatest thickness. We can attribute this thickness to the 3 hours of draining time and the appearance of two layers, one from each of the 2 cycles of the draining/annealing process. Peiró et al. [15] reported TiO_2 thin films of 54 nm by the drain coating method, with a draining time of 5 minutes in the colloidal solution.

3.2. Photoactive Films (TiO_2/UV) Test Evaluation

3.2.1. Dissolved Oxygen Concentration. In photocatalysis, reduction and oxidation processes occur under oxygenated conditions, improving the photocatalytic activity and promoting e^-/h^+ pair generation; additionally, oxygen is an electron acceptor generated in TiO_2, and it is reduced to $O_2^{\bullet-}$, H_2O_2, OH radicals and Ti-$O^\bullet$ (Ti-$^\bullet$OH), all of which enable the photocatalytic oxidation of organic compounds. O_2 can also react with organic radicals to form $ROO^\bullet$. The dissolved oxygen concentration (DO) in solution for different experimental designs was between 0.92 mg L^{-1} and 2.30 mg L^{-1}. The maximum DO obtained was below other values reported (6 to 40 mg L^{-1}) for related compounds during degradation studies [22–26], which also had a high level of mineralization. In films obtained after 2 hours of draining, a slightly decreased tendency toward ROS formation was observed. These results indicate that complete mineralization did not occur during the course of the assay, as consumption of the dissolved oxygen was not observed.

3.2.2. Determination of $O_2^{\bullet-}$ and Endosulfan Degradation. Figure 4 shows the behavior of the $O_2^{\bullet-}$ radicals that were generated. To monitor these radicals, lucigenin was employed to react with the superoxide anion radical $O_2^{\bullet-}$, resulting in release of a photon [18]. High levels of free radical detection are thought to indicate high level of pesticide elimination;

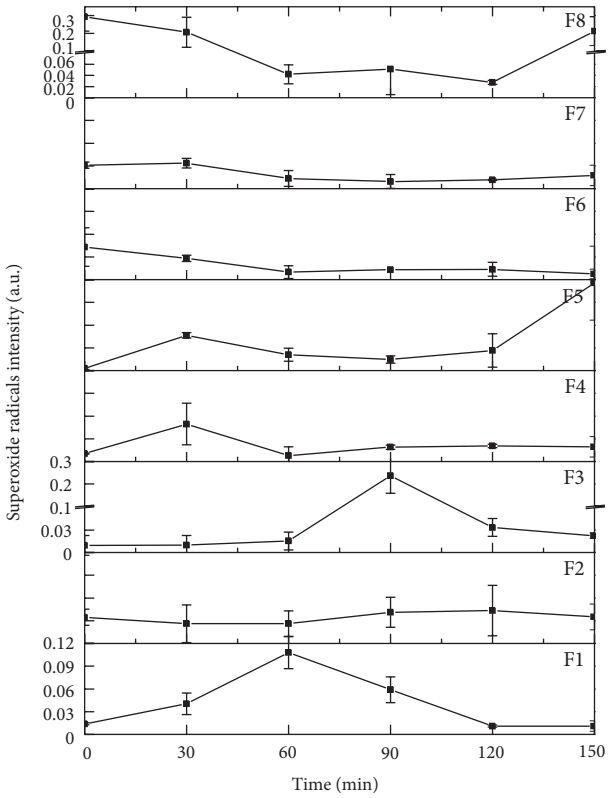

Figure 4: Superoxide radicals intensities during photoactivity assays (TiO_2/UV) employing 2^3 factorial experimental design.

however, this behavior was not observed. Instead, in treatments that showed the highest free radical response, a low endosulfan concentration was observed (F3, F4, and F8). However, in F6 treatment, a negative correlation ($R^2 = 0.7$; $P > 0.01$) between superoxide radicals and pesticide degradation was observed; therefore, we believe that the low levels of superoxide radicals detected were due to ROS-pollutant oxidation reactions. No correlation between the levels of dissolved oxygen and superoxide radicals was observed.

Assays with films F2, F5, and F6 showed lower initial endosulfan adsorptions relative to other films. However, all tests show pesticide concentrations above the theoretical amount added (Figure 5).

The ANOVA indicates that total endosulfan reduction ($\alpha + \beta$) with a photocatalytic system (TiO_2/UV) was significantly affected ($P < 0.05$) by the draining time of the films. The regression analysis model showed a depletion of endosulfan after 2 hours of draining time. The dissolved oxygen concentration during preparation of the photocatalytic system had no effect on the TiO_2 film preparation conditions. Otherwise, the annealing temperature of the films was statistically significant ($P > 0.05$) for superoxide radical generation and for the interaction between *C*-IT and *C*-IT-*T* (Table 3).

Table 3: Analysis of variance (ANOVA) for superoxide radical generation in photoactivity assays (TiO_2/UV) at maximum total endosulfan degradation.

Factor	DF	Mean Sqr	*F* value	Pr > *F*
Cycles (*C*)	1	0.0019	1.55	0.2478
Immersion time (IT)	1	0.0039	3.20	0.1116
Temperature (*T*)	1	0.0207	16.78	0.0035
C-IT	1	0.0163	13.25	0.0066
C-T	1	0.0005	0.42	0.5350
IT-*T*	1	0.0044	3.62	0.0937
C-IT-*T*	1	0.0239	19.44	0.0023

A regression analysis (5) showed an increase of $O_2^{\bullet-}$ radicals at high temperatures (550°C) and the interaction between C-IT-T and C-IT. Consider

$$O_2^{\bullet-} \text{ radicals} = 0.058 + 0.01C + 0.02\text{IT} + 0.04T + 0.03C\text{-IT} + 0.01C\text{-}T + 0.017T\text{-}T + 0.04C\text{-IT-}T. \quad (5)$$

The regression analysis indicated that superoxide radical generation and endosulfan reduction increased with larger numbers of draining/annealing cycles and higher annealing temperature at 30 minutes of the assay (Figure 6). Meanwhile, β-endosulfan (βE) degradation was affected by a large number of cycles, high draining time, and high annealing temperature. Nevertheless, dissolved oxygen concentrations decreased with increases in the draining time (2 h) and high annealing temperatures (550°C).

The conditions employed for film preparation affected the photocatalytic activities of the eight films prepared, as demonstrated by the rates of endosulfan reduction, the metabolites produced and the αE and βE residuals that were detected after 150 min; we obtained a total endosulfan photodegradation of 78.8%, 77.2%, and 70.7% with films F6, F5, and F2, respectively. However, the highest photoactivity (78.8%) of all treatments was obtained at 30 min with film F6 (2 h draining time, 2 cycles of draining/annealing at 550°C). In addition, photocatalysis adsorption/desorption processes were involved in endosulfan reduction, mainly with the F4, F8, F7 and F5 films. In the latter case, an apparent high removal of βE (81.9%) and total endosulfan (77.2%) was observed after 90 minutes. The adsorption/desorption of endosulfan might be related to the higher thickness of films F8, F3, F6, and F4 in comparison to films F2, F1, and F5 (Table 2). These thickness values are still high relative to those obtained by Peiró et al. [15], who used a shorter draining time (5 minutes). However, the high thickness of the photocatalyst was effective as demonstrated by the percentage of endosulfan reduction and the metabolites identified.

The main endosulfan metabolites produced by photocatalysis, which were detected in all treatments, were alcohol endosulfan (AlE), ether endosulfan (EE), and lactone endosulfan (LE) and the parental compounds α-endosulfan (αE), and β-endosulfan (βE). The highest production levels for AlE (in mg L^{-1}) were 1.46 ± 0.010, 0.863 ± 0.389, 0.784 ± 0.064,

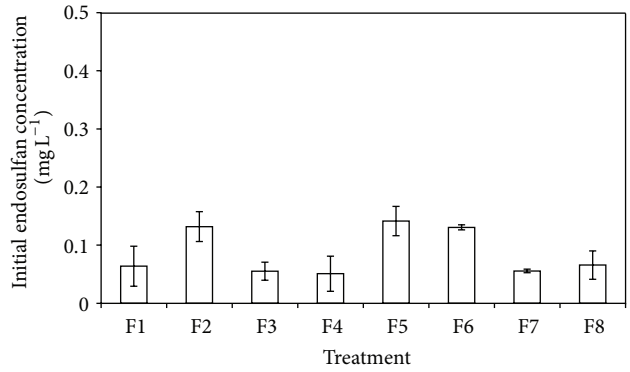

Figure 5: Initial endosulfan concentration in photoactivity assays employing 2^3 factorial experimental design.

Table 4: Kinetic reaction constants, maximum time and total endosulfan degradation during photoactivity assays (TiO_2/UV).

Films	α-Endosulfan			β-Endosulfan			Total endosulfan		
	K_{app}	r^2	T_{max} (min) (% R_{max})	K_{app}	r^2	T_{max} (min) (% R_{max})	K_{app}	r^2	T_{max} (min) (% R_{max})
F1	0.0048	0.82	120 (40)	0.0058	0.92	120 (45.4)	0.0053	0.89	120 (42.9)
F2	0.0080	0.93	150 (67.9)	0.0060	0.86	150 (62.5)	0.0086	0.945	150 (70.7)
F3	0.0035	0.45	120 (50.7)	0.0041	0.53	120 (52.9)	0.0035	0.475	120 (46.1)
F4	ws	ws		ws	ws		ws	ws	
F5	0.0055	0.80	90 (47.8)	0.0115	0.86	90 (81.9)	0.0163	0.99	90 (77.2)
F6	0.0101	0.94	30 (78.4)	0.0079	0.97	30 (70.1)	0.0102	0.93	30 (78.8)
F7	ws	ws		ws	ws		ws	ws	
F8	ws	ws		ws	ws		ws	ws	

ws: without setting.

0.747 ± 0.010, 0.708 ± 0.013, and 0.445 ± 0.297 with films F3, F6, F4, F7, F2, and F1, respectively.

The residuals αE and βE (in mg L^{-1}) were (0.053 ± 0.013 and 0.051 ± 0.007), 0.021 ± 0.009 and 0.018 ± 0.008 and 0.017 ± 0.009 and 0.015 ± 0.008 with films F3, F6 and F1 (Figure 7).

The first endosulfan metabolite, sulfate endosulfan, was not detected, which agrees with the results of Archer et al. [27] who noted that this compound was not identified as a photodecomposition product and that no degradation products were produced when it was irradiated.

3.2.3. Determination of Endosulfan Degradation Rate. The rates of disappearance of the primary substrates through heterogeneous photocatalysis are described by the kinetic model of Langmuir-Hinshelwood [28, 29]:

$$r = \frac{dC}{dt} = \frac{kKC}{1 + KC}, \tag{6}$$

where r is the reaction rate in terms of the reactant concentration (mg L^{-1} min^{-1}), C is the concentration of reactant (mg L^{-1}), t is the radiation time (min), k is the reaction rate constant (mg L^{-1} min^{-1}), and K is the reactant adsorption coefficient (L mg^{-1}). The value of k_{app} is a constant for certain systems and solutes; k will be linearly dependent on UV light intensity [29]. If the initial concentration is millimolar, the following can be set to a first-order model [2]:

$$\ln \frac{C_0}{C} = kKt = k_{app}t, \tag{7}$$

where k_{app} (min^{-1}) is the first order constant. A high k_{app} value will indicate a higher rate of pollutant removal. The treatments involving films F5 and F6 showed the highest kinetic constant for α-endosulfan and β-endosulfan, both with acceptable model settings (Table 4), but the rate of degradation will strongly depend on the photocatalysis conditions. Regarding this finding, kinetic constants were reported in the range of 0.007 to 0.096 min^{-1} for photocatalytic treatments of dyes [30–33]; in particular, Da silva and Faria [34] reported k_{app} values for four nitrogen herbicides between 0.069 and 0.096 min^{-1}.

However, the maximum degradation percentage reached, as well as a high kinetic constant, is important; together, these factors would indicate pollutant removal over short periods of time, as in our case, where after 30 min, we obtained the maximum degradation using film F6 (Figure 8). The treatments with films F6, F5 and F2 yielded an acceptable percentage of photodegradation of the total pesticide. Outstanding results were obtained for treatments with film F6 after 2 cycles of draining for 2 hours with an annealing temperature of

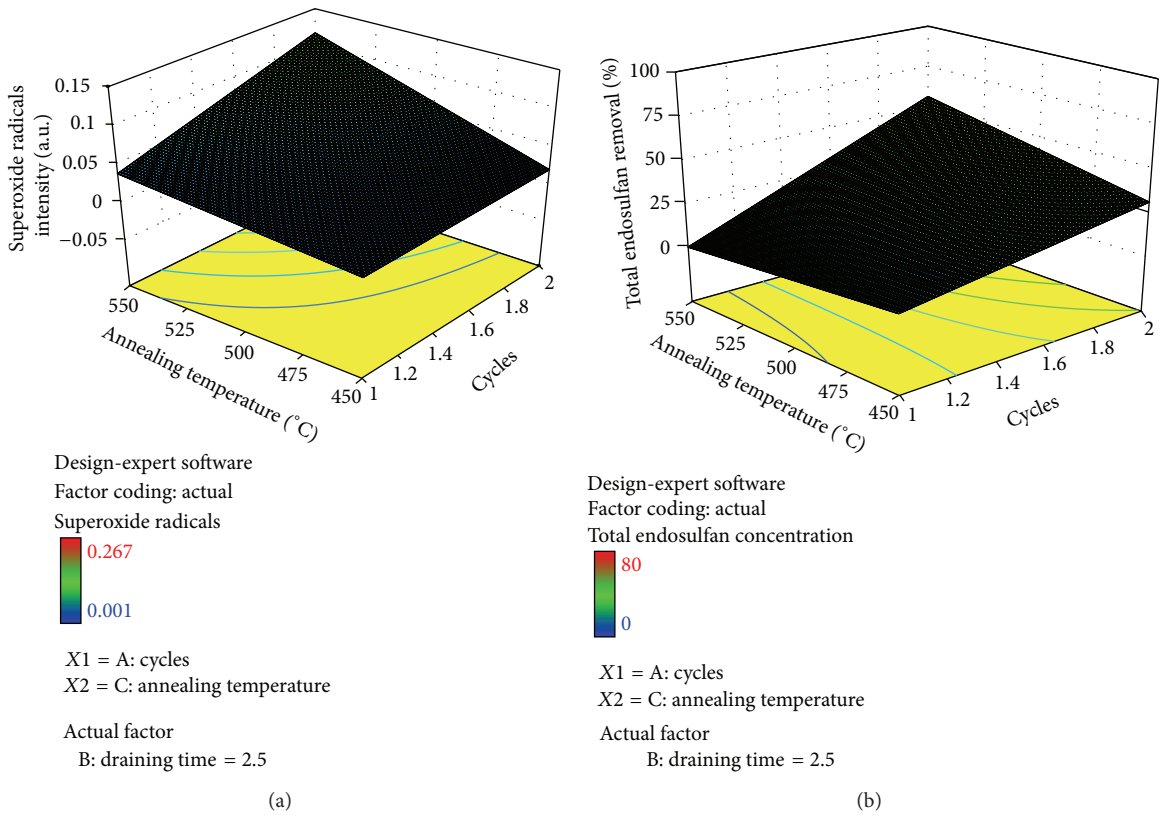

FIGURE 6: Effect of high level of draining/annealing cycles and annealing temperature for (a) superoxide radical generation; and (b) total endosulfan degradation at 30 minutes of the photoactivity assay.

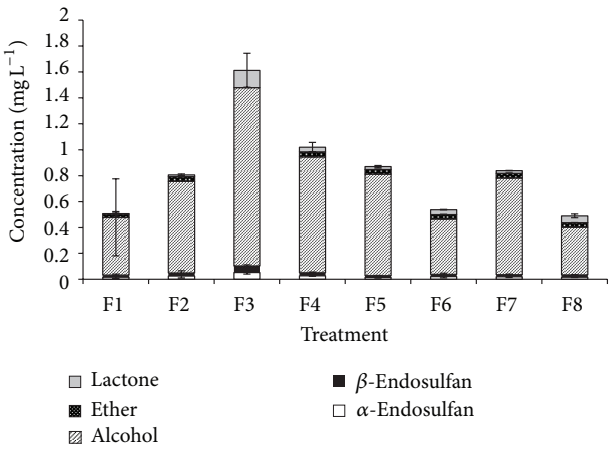

FIGURE 7: Residual endosulfan and its metabolites produced at 150 minutes in photoactivity assays (TiO_2/UV). (gray square) Lactone, (dotet square) ether, (line square) alcohol, (black square) β-endosulfan and (white square) α-endosulfan.

550°C. These conditions resulted in 78.8% total endosulfan degradation and a high efficiency.

3.3. Dark Phase (TiO_2) Control. In these assays, we refer to endosulfan disappearance by adsorption/desorption processes with TiO_2 films due to the lack of appropriate conditions to support photocatalytic processes. The treatments using films F2 and F6 (both with 2 cycles of draining/annealing) showed an adsorption equilibrium, with an increase at the end of the treatment. The treatment with film F3 presented an adsorption/desorption equilibrium after 90 minutes, at which point the concentrations of the α and β pesticide isomers remain constant. Treatments with films F4 and F5 reached equilibrium after 120 and 60 minutes, respectively. Treatments with film F6 showed equilibrium until the 180 minute time point, after which the endosulfan concentration increased. During treatments with film F7, equilibrium was reached at 90 minutes. Treatment with film F8 did not result in an adsorption/desorption equilibrium because no constant tendency was observed (Figure 8).

The total endosulfan concentrations present are similar for each endosulfan isomer (α and β) after deducting the adsorption/desorption equilibrium times when the concentration does not change. Once this state is attained the photocatalytic process should begin because the pollutant molecules are in the surface TiO_2 adsorption sites [34]. At this point, the quantity of the adsorbed molecules in the photocatalyst can be calculated by [35]

$$n = \frac{C_{in} - C_{eq}}{C_{TiO_2}}, \tag{8}$$

where C_{in} is the initial pollutant concentration, C_{eq} is the equilibrium pollutant concentration, and C_{TiO_2}

Table 5: Adsorption equilibrium parameters in dark phase control with TiO_2 films formed using the 2^3 experimental design.

Treatment	C_{eq} (mg L^{-1})	T_{eq} (min)	n ($\times 10^{-5}$ mol cm^{-3})
F1	0.035 ± 0.010	120	0.288
F2	0.032 ± 0.004	30	0.323
F3	0.040 ± 0.007	90	1.820
F4	0.039 ± 0.006	120	2.89
F5	0.045 ± 0.017	60	11.20
F6	0.047 ± 0.017	30	0.414
F7	0.033 ± 0.006	90	—
F8	we	we	—

we: without equilibrium.

is the quantity of TiO_2 deposited. We performed this calculation using the volume of the TiO_2 films rather than the weight of the TiO_2 deposited; thus, the units of n will be mol cm^{-3} (Table 5). Film F7 showed an irregular profilometer structure; thus, the thickness was not obtained, and the number of moles of endosulfan adsorbed was not calculated.

The highest endosulfan degradations were for films F6 (78.8%) > F5 (77.2%) > F2 (70.7%), and the same tendency was observed in films thickness F6 (8.21 μm)> F5 (4.29 μm) > F2 (2.02 μm). In these treatments, no pesticide desorption (increase of endosulfan concentration in solution) was observed. However, a higher pesticide adsorption by the thinnest TiO_2 films was expected and therefore an increase of the photocatalytic degradation, as it was reported by Negishi et al. [36], since they observed changes in photocatalytic ability with film thickness; this effect was not observed in films F6, F5, and F2 (Table 5), as the film with the highest pesticide degradation efficiency (F6) did not show the highest film adsorption, in terms of moles of endosulfan n.

The intensity response of the free $O_2^{-\bullet}$ radicals was lower than in the light phase given the absence of a source of reactive species, UV light. The total endosulfan volatilization was minimal in units of ng mL^{-1} and constant. No detectable quantities of the pesticide metabolites were determined in the dark phase experimental design.

Differences in the initial total endosulfan concentration in the light and dark phases were observed due to pollutant solubility and the adsorption phenomena in the system.

3.4. Photolysis Control (UV). In the photolysis process, superoxide radical generation can occur, as well as intermolecular rearrangements or molecular excitation that can be involved in secondary reactions [37, 38]. Such reactions have a marked dependence on dissolved oxygen in the system. Mineralization during photolysis was not observed. Otherwise, an increase in the concentration of DO was observed in the range from 1.05 to 1.60 mg L^{-1}.

The superoxide radical $O_2^{-\bullet}$ showed a maximum response at 120 minutes with a similar tendency but a low intensity of TiO_2/UV. At the end of the treatment,

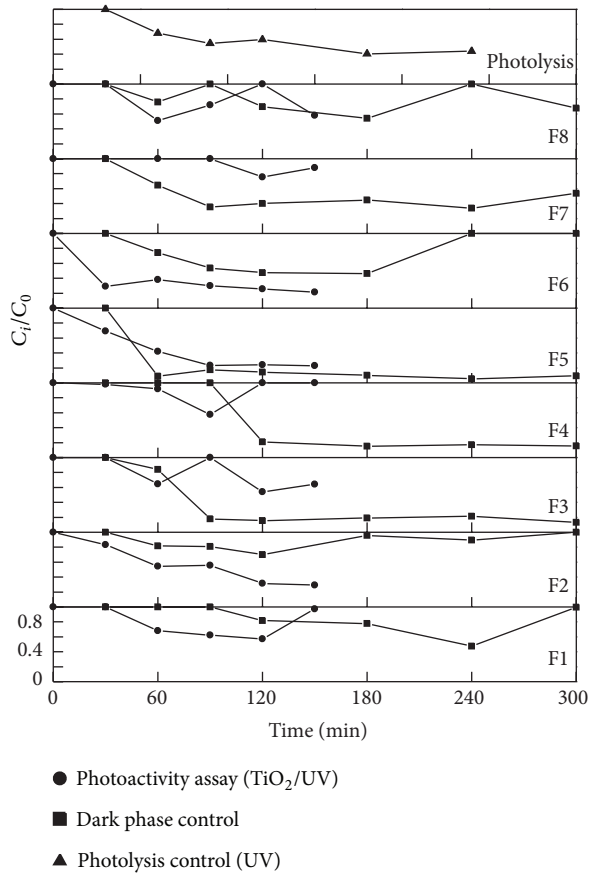

Figure 8: Total endosulfan concentration during assays. Photoactivity assay (mg L^{-1}) $C_{0/F2,F5,F6}$ = 0.0135 ± 0.006, $C_{0/F1,F3,F4,F7,F8}$ = 0.058 ± 0.006. Dark phase control (mg L^{-1}) $C_{0/F3,F4}$ = 0.2285 ± 0.006, $C_{0/F1,F2,F5,F6,F7,F8}$ = 0.056 ± 0.019.

the response in radicals was significantly different from that of film F8 ($P > 0.05$). The total endosulfan degradation rate was 0.0053 min^{-1}, with approximately 0.84 of the Langmuir-Hishelwood model. The k_{app} was lower than that observed in photocatalytic treatments with films F2, F5, and F6 (Figure 8).

After 30 minutes of treatment, the photolysis experiment showed a significantly lower total endosulfan degradation than that observed with film F6, and no significant difference was observed relative to other photocatalytic treatment films.

We suggest that the photocatalytic degradation of endosulfan in an assay with film F2 is due to photolysis because positive Pearson's correlation was determined ($R^2 = 0.79$, $P > 0.002$). The LSD test showed a critical value of $t = 4.3$, and there are no significant differences in the kinetics of film F2 in terms of the photolysis during degradation.

4. Conclusions

The films prepared under our 2^3 factorial experimental design conditions using the drain coating method affected the photoactivity properties of the films, despite the thickness of the films (2.02 (F2) to 17.19 μm (F8)). The photoactivity of all

TiO_2 films, except F7, which may be due to the photoactive TiO_2 phase, was supported by the Raman spectra which displayed the bands characteristic of anatase.

The draining time, annealing temperature, and number of cycles affect the photoactivity of the TiO_2 films in terms of endosulfan degradation, which was highest (77.2% and 78.8%) with TiO_2 films grown at an annealing temperature of 550°C (F5 and F6) for 90 or 30 minutes. Such treatments result in the most efficient photoreaction rates in comparison to other films obtained under different conditions of our 2^3 factorial experimental design, including photolysis (UV radiation) and equilibrium adsorption/desorption at 30 minutes. The difference in the initial concentration of pesticide may be due to its low solubility and rapid adsorption onto films. The endosulfan pesticide volatilization and film adsorption was low (ng mL^{-1} cm^{-3}) throughout the treatments.

The metabolites produced included alcohol endosulfan, ether, and lactone endosulfan, each of which was detected in all light phase experimental conditions. Alcohol endosulfan products were produced in higher concentrations than were the ether or lactone endosulfan products.

Acknowledgments

The authors are grateful to Consejo Nacional de Ciencia y Tecnología (CONACyT, Grant 203849) and to Instituto de Ciencia y Tecnología del Distrito Federal (ICyTDF, Grant PICSO10-51) for their finantial support of this work and to Professors Juan Manriquez and Jesús Pérez Bueno from Centro de Investigación y Desarrollo Tecnológico en Electroquímica S.C. for providing a Raman Microscope and profilometer, respectively.

References

[1] D. Y. Goswami, "A review of engineering developments of aqueous phase solar photocatalytic detoxification and disinfection processes," *Journal of Solar Energy Engineering*, vol. 119, no. 2, pp. 101–107, 1997.

[2] I. A. Alaton and I. A. Balcioglu, "Photochemical and heterogeneous photocatalytic degradation of waste vinylsulphone dyes: a case study with hydrolyzed reactive black 5," *Journal of Photochemistry and Photobiology A*, vol. 141, no. 2-3, pp. 247–254, 2001.

[3] A. Alinsafi, F. Evenou, E. M. Abdulkarim et al., "Treatment of textile industry wastewater by supported photocatalysis," *Dyes and Pigments*, vol. 74, no. 2, pp. 439–445, 2007.

[4] C. Shifu and C. Gengyu, "Photocatalytic degradation of organophosphorus pesticides using floating photocatalyst $TiO_2{\cdot}SiO_2$/beads by sunlight," *Solar Energy*, vol. 79, no. 1, pp. 1–9, 2005.

[5] S. Ahmed, M. G. Rasul, W. N. Martens, R. Brown, and M. A. Hashib, "Advances in heterogeneous photocatalytic degradation of phenols and dyes in wastewater: a review," *Water, Air, and Soil Pollution*, vol. 215, no. 1–4, pp. 3–29, 2011.

[6] D. S. Bhatkhande, V. G. Pangarkar, and A. A. C. M. Beenackers, "Photocatalytic degradation for environmental applications—a review," *Journal of Chemical Technology and Biotechnology*, vol. 77, no. 1, pp. 102–116, 2002.

[7] J. Weber, C. J. Halsall, D. Muir et al., "Endosulfan, a global pesticide: a review of its fate in the environment and occurrence in the Arctic," *Science of the Total Environment*, vol. 408, no. 15, pp. 2966–2984, 2010.

[8] V. Laabs, A. Wehrhan, A. Pinto, E. Dores, and W. Amelung, "Pesticide fate in tropical wetlands of Brazil: an aquatic microcosm study under semi-field conditions," *Chemosphere*, vol. 67, no. 5, pp. 975–989, 2007.

[9] J. M. Herrmann, "Heterogeneous photocatalysis: fundamentals and applications to the removal of various types of aqueous pollutants," *Catalysis Today*, vol. 53, no. 1, pp. 115–129, 1999.

[10] A. Fujishima, T. N. Rao, and D. A. Tryk, "Titanium dioxide photocatalysis," *Journal of Photochemistry and Photobiology C*, vol. 1, no. 1, pp. 1–21, 2000.

[11] A. Sobczyński and A. Dobosz, "Water purification by photocatalysis on semiconductors," *Reviews Polish Journal of Environmental Studies*, vol. 10, no. 4, pp. 195–205, 2001.

[12] I. K. Konstantinou and T. A. Albanis, "Photocatalytic transformation of pesticides in aqueous titanium dioxide suspensions using artificial and solar light: intermediates and degradation pathways," *Applied Catalysis B*, vol. 42, no. 4, pp. 319–335, 2003.

[13] R. Andreozzi, V. Caprio, A. Insola, and R. Marotta, "Advanced oxidation processes (AOP) for water purification and recovery," *Catalysis Today*, vol. 53, no. 1, pp. 51–59, 1999.

[14] S. Devipriya and S. Yesodharan, "Photocatalytic degradation of pesticide contaminants in water," *Solar Energy Materials and Solar Cells*, vol. 86, no. 3, pp. 309–348, 2005.

[15] A. Peiró, J. Peral, C. Domingo, X. Doménech, and J. A. Ayllón, "Low-temperature deposition of TiO_2 thin films with photocatalytic activity from colloidal anatase aqueous solutions," *Chemistry of Materials*, vol. 12, no. 8, pp. 2567–2573, 2001.

[16] Y. Sakatani, D. Grosso, L. Nicole, C. Boissière, G. J. D. A. A. Soler-Illia, and C. Sanchez, "Optimised photocatalytic activity of grid-like mesoporous TiO_2 films: effect of crystallinity, pore size distribution, and pore accessibility," *Journal of Materials Chemistry*, vol. 16, no. 1, pp. 77–82, 2006.

[17] A. Peiró, E. Brillas, J. Peral, X. Doménech, and J. A. Ayllón, "Electrochemically assisted deposition of titanium dioxide on aluminium cathodes," *Journal of Materials Chemistry*, vol. 12, no. 9, pp. 2769–2773, 2002.

[18] G. P. Bolwell, D. R. Davies, C. Gerrish, C. K. Auh, and T. M. Murphy, "Comparative biochemistry of the oxidative burst produced by rose and French bean cells reveals two distinct mechanisms," *Plant Physiology*, vol. 116, no. 4, pp. 1379–1385, 1998.

[19] Secretary of Economy, "Water analysis—determination of dissolved oxygen in natural, wastewaters and wastewaters treated—test method," NMX-AA-012-SCFI-2001, 2001.

[20] J. V. Hinshaw, "Solid phase microextraction," *LC&GC*, no. 16, pp. 803–807, 2003.

[21] A. Felske and W. J. Plieth, "Raman spectroscopy of titanium dioxide layers," *Electrochimica Acta*, vol. 34, no. 1, pp. 75–77, 1989.

[22] M. Subramanian and A. Kannan, "Effect of dissolved oxygen concentration and light intensity on photocatalytic degradation of phenol," *Korean Journal of Chemical Engineering*, vol. 25, no. 6, pp. 1300–1308, 2008.

[23] T. Hirakawa, C. Koga, N. Negishi, K. Takeuchi, and S. Matsuzawa, "An approach to elucidating photocatalytic reaction mechanisms by monitoring dissolved oxygen: effect of H_2O_2 on photocatalysis," *Applied Catalysis B*, vol. 87, no. 1-2, pp. 46–55, 2009.

[24] C. S. Zalazar, C. A. Martin, and A. E. Cassano, "Photocatalytic intrinsic reaction kinetics—II: effects of oxygen concentration on the kinetics of the photocatalytic degradation of dichloroacetic acid," *Chemical Engineering Science*, vol. 60, no. 15, pp. 4311–4322, 2005.

[25] C. B. Almquist and P. Biswas, "A mechanistic approach to modeling the effect of dissolved oxygen in photo-oxidation reactions on titanium dioxide in aqueous system," *Chemical Engineering Science*, vol. 56, no. 11, pp. 3421–3430, 2001.

[26] B. Kraeutler and A. J. Bard, "Heterogeneous photocatalytic decomposition of saturated carboxylic acids on TiO_2 powder. Decarboxylative route to alkanes," *Journal of the American Chemical Society*, vol. 100, no. 19, pp. 5985–5992, 1978.

[27] T. E. Archer, I. K. Nazer, and D. G. Crosby, "Photodecomposition of endosulfan and related products in thin films by ultraviolet light irradiation," *Journal of Agricultural and Food Chemistry*, vol. 20, no. 5, pp. 954–956, 1972.

[28] I. K. Konstantinou and T. A. Albanis, "TiO_2-assisted photocatalytic degradation of azo dyes in aqueous solution: kinetic and mechanistic investigations: a review," *Applied Catalysis B*, vol. 49, no. 1, pp. 1–14, 2004.

[29] J. Thomas, K. P. Kumar, and K. R. Chitra, "Synthesis of ag doped nano TiO_2 as efficient solar photocatalyst for the degradation of endosulfan," *Advanced Science Letters*, vol. 4, no. 1, pp. 108–114, 2011.

[30] A. Vidal, "Developments in solar photocatalysis for water purification," *Chemosphere*, vol. 36, no. 12, pp. 2593–2606, 1998.

[31] M. Stylidi, D. I. Kondarides, and X. E. Verykios, "Pathways of solar light-induced photocatalytic degradation of azo dyes in aqueous TiO_2 suspensions," *Applied Catalysis B*, vol. 40, no. 4, pp. 271–286, 2003.

[32] G. A. Epling and C. Lin, "Photoassisted bleaching of dyes utilizing TiO_2 and visible light," *Chemosphere*, vol. 46, no. 4, pp. 561–570, 2002.

[33] K. Tanaka, K. Padermpole, and T. Hisanaga, "Photocatalytic degradation of commercial azo dyes," *Water Research*, vol. 34, no. 1, pp. 327–333, 2000.

[34] C. G. da Silva and J. L. Faria, "Photochemical and photocatalytic degradation of an azo dye in aqueous solution by UV irradiation," *Journal of Photochemistry and Photobiology A*, vol. 155, no. 1-3, pp. 133–143, 2003.

[35] S. Parra, J. Olivero, and C. Pulgarin, "Relationships between physicochemical properties and photoreactivity of four biorecalcitrant phenylurea herbicides in aqueous TiO_2 suspension," *Applied Catalysis B*, vol. 36, no. 1, pp. 75–85, 2002.

[36] N. Negishi, K. Takeuchi, and T. Ibusuki, "Surface structure of the TiO_2 thin film photocatalyst," *Journal of Materials Science*, vol. 33, no. 24, pp. 5789–5794, 1998.

[37] A. Gora, B. Toepfer, V. Puddu, and G. Li Puma, "Photocatalytic oxidation of herbicides in single-component and multicomponent systems: reaction kinetics analysis," *Applied Catalysis B*, vol. 65, no. 1-2, pp. 1–10, 2006.

[38] G. Grabner and C. Richard, "Mechanisms of direct photolysis of biocides based on halogenated phenols and anilines," in *The Handbook Environmental Chemistry: Part 2*, vol. 2, pp. 161–192, Springer, Berlin, Germany, 2005.